

Visualizing influence of point defects on electronic band structure of graphene

M. Farjam*

School of Nano-Science, Institute for Research in Fundamental Sciences (IPM), P.O. Box 19395-5531, Tehran, Iran

(Dated: March 27, 2025)

The supercell approach, commonly used in electronic structure calculations of defective crystals, results in complicated energy bands because of inevitable zone folding. We describe ways of improving visualization of band structure data, based on unfolded spectral weights and partial orbital populations, which are obtained in this work from density-functional based tight-binding method. By applying these ideas to supercells of graphene with different types of point defects, we obtain band structures which are easier to understand, and to compare with angle-resolved photoemission spectra.

PACS numbers: 71.20.-b, 73.20.Hb, 73.22.Pr, 79.60.-i

I. INTRODUCTION

The electronic band structure of a crystal is an important tool to understand its electronic, optical, transport and magnetic properties. Thus, the band structure of graphene shows that it is a semiconductor with a gapless spectrum, where the valence and conduction bands meet at only two inequivalent points in k space, and the low-energy excitations have linear dispersion, characteristic of massless Dirac fermions.^{1,2} Electronic properties of graphene have attracted great attention since the announcement of the first experiments on this two-dimensional (2D) crystal.³⁻⁵

Defects and impurities have a significant influence on the electronic properties of semiconductors, and can be introduced deliberately to tailor their electronic structure. In graphene, atomic impurities, point and line defects, edges and substrates can all modify the electronic structure in important ways. Two simple impurities are substitutional dopants formed by carbon neighbors in the periodic table, boron and nitrogen, which can turn graphene into a p- or n-type semiconductor, respectively.⁶ The simplest defects are vacancies and hydrogen adsorbates, which induce midgap states and magnetic moments in graphene.⁷

A convenient way of treating point defects is via the supercell approach, within density-functional theory (DFT) or tight-binding method calculations. The supercell device allows us to use methods designed for periodic structures to treat relatively isolated defects. There is a disadvantage, however, in that the Brillouin zone (BZ) shrinks in proportion to the size of the supercell. The folded bands obtained from supercell calculations become complicated to understand, and difficult to compare with angle-resolved photoemission spectroscopy (ARPES) experiments. This often leaves the density of states (DOS) as the sole option for spectral analysis.

However, there are ways to improve visualization of band structures. A simplification is made possible by the unfolding method, which allows plotting effective bands in the larger BZ of the normal system, i.e., one described in terms of the primitive unit cell.⁸⁻¹² Furthermore, an enhancement can be made by incorporating orbital con-

tributions in both supercell and normal cell band structures. The orbital decomposition is more commonly used in obtaining partial density of states (PDOS), but it can be applied to band structure plots as well.¹³ In this paper, we develop ways of implementing the above ideas in the visualization of electronic structure data. We then apply them to the case of graphene containing point defects. We present density-functional based tight-binding (DFTB) calculations for 5×5 supercells of graphene containing a nitrogen impurity, a hydrogen adsorbate, and a vacancy, respectively.

In Sec. II we describe the computational details, and in Sec. III we present and discuss the results of our calculations.

II. COMPUTATIONAL DETAILS

A. DFTB calculations

We calculate the prerequisite electronic structure data for the unfolding method by the DFTB+ code,¹⁴ which is an efficient and accurate implementation of the DFTB method.¹⁵ Since the method is based on a small set of non-orthogonal atomic orbitals, $2s$, $2p_x$, $2p_y$, and $2p_z$, for carbon and nitrogen, and $2s$ for hydrogen, it is also quite suitable for the unfolding formula to be described below.

We use $n \times n$ supercells, which encompass $N_p = n^2$ normal unit cells, or $2n^2$ honeycomb lattice sites. This represents, for $n = 5$ in our examples, a 2% concentration of periodically arranged point defects, which is sufficiently small for them to be considered as relatively isolated, but large enough to produce visible effects. We need to run the code several times. Having defined a supercell with our choice of defect placed in a tentative position, in a first calculation we allow the atomic positions to relax. Then using the optimized coordinates, we calculate the DOS and PDOS using a finer k -mesh for the desired accuracy. Finally, we use the charge saved from the previous self-consistent calculation to obtain the data for the band structure along the given paths in supercell and normal cell Brillouin zones, respectively.

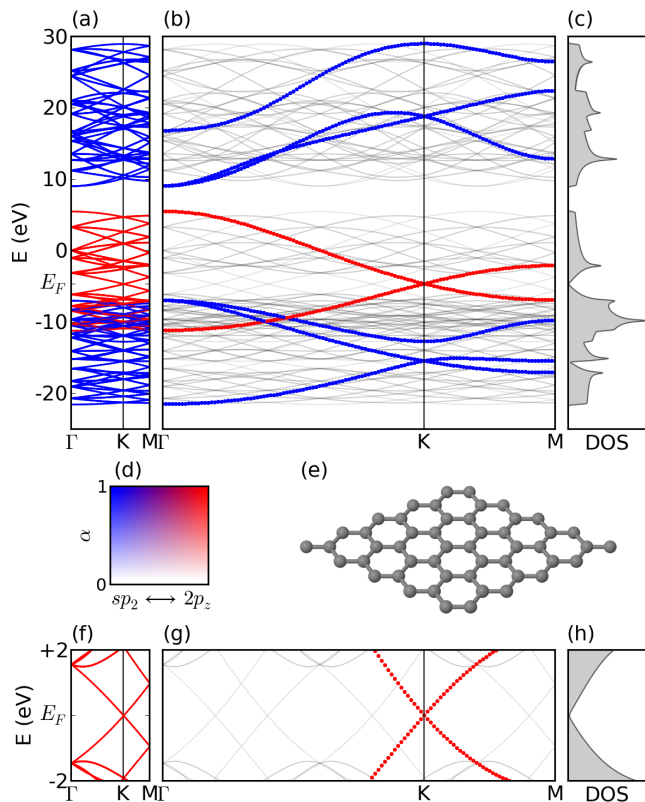


FIG. 1. (Color online) (a) Band structure of graphene obtained from supercell calculations. (b) Unfolded bands in the normal Brillouin zone. The light gray bands are supercell band structure in extended zone. (c) Total DOS. (d) Color map used in band structure plots. (e) The 5×5 unit cell used in supercell calculations. (f–h) Band structure and DOS limited to a window of $E_F \pm 2$ eV centered on the Dirac point.

The basic ingredients needed for the unfolding method consist of eigenvector coefficients and overlap integrals. Thus concomitant with the band structure calculations, we instruct the code to save these data in designated files. To estimate the size of the data, which may grow quite large, let N_b be the total number of orbitals in a supercell, which is also the total number of bands, and let N_k be the number of k points used in the calculation of the band structure. The overlap integrals are represented as a sparse matrix,¹⁴ so their size can be estimated to be less than $N_R \times N_b \times N_b$ real numbers, where N_R is the few number of unit cells required to include nonzero overlaps. On the other hand, the total size of the complex eigenvectors, which is by far the larger set of data, is exactly $2 \times N_k \times N_b \times N_b$ real numbers.

B. Unfolding procedure

We need an unfolding formula that takes into account non-orthogonality of atomic orbitals. Such a formula has been derived recently by C.-C. Lee *et al.* in Ref. 11. Here,

we describe the method in some detail in order to further elucidate its numerical implementation.

Following custom, we use upper and lower cases to refer to supercell and normal cell variables, respectively, so \mathbf{K} and \mathbf{k} denote the wavevectors of the supercell Brillouin zone (SBZ) and normal cell Brillouin zone (NBZ), respectively. A given \mathbf{k} in NBZ folds onto exactly one \mathbf{K} in SBZ but, in contrast, each \mathbf{K} unfolds back to N_p normal system \mathbf{k} vectors in NBZ. The unfolding method consists of assigning the same energy at a given \mathbf{K} to the multiple unfolded \mathbf{k} 's with suitable spectral weights. However, in practice, we use a simplified procedure. If we choose a k path in the NBZ, and regard it as a path in the extended zone of the supercell, then each \mathbf{K} needs to be ‘unfolded’ to only a single $\mathbf{k} = \mathbf{K}$. We then calculate the energy eigenvalues along this path for the supercell system, and determine their spectral weights by the unfolding formula.

It is useful to note some properties of non-orthogonal orbitals. The normalization of an eigenvector, $|\mathbf{K}J\rangle$, in terms of its expansion coefficients, is given by

$$\sum_{MN} C_N^{\mathbf{K}J*} S_{NM}(\mathbf{K}) C_M^{\mathbf{K}J} = 1, \quad (1)$$

where $S(\mathbf{K})$ is the overlap matrix of Bloch orbitals,

$$S_{NM}(\mathbf{K}) = \sum_{\mathbf{R}} e^{i\mathbf{K}\cdot\mathbf{R}} S_{NM}(\mathbf{R}), \quad (2)$$

and the overlap integrals are defined by

$$S_{NM}(\mathbf{R}) \equiv S_{0N,\mathbf{R}M} = \langle 0N | \mathbf{R}M \rangle. \quad (3)$$

In Eq. (1), J and N are band and orbital indices, respectively, and are both in the range of 1 to N_b . Breaking down the contributions in Eq. (1), we can write the (Mulliken) orbital populations for an eigenstate as

$$P_N^{\mathbf{K}J} = \Re \left\{ C_N^{\mathbf{K}J*} \sum_M S_{NM}(\mathbf{K}) C_M^{\mathbf{K}J} \right\}. \quad (4)$$

The unfolding procedure must uncover the hidden translational symmetry inherited by the supercell system from the normal system. A useful connection between the two systems is expressed by the Fourier relation,⁸

$$\frac{1}{N_p} \sum_{\mathbf{G}} e^{i\mathbf{G}\cdot\mathbf{r}} = \delta_{\mathbf{r},\mathbf{R}}, \quad (5)$$

where \mathbf{R} and \mathbf{r} are the corresponding lattice vectors, respectively, and the sum is over the set of N_p reciprocal lattice vectors of the supercell system that unfold the SBZ onto the NBZ. An orbital described in the supercell system by the pair \mathbf{R}, M can be described in the normal system through the mapping¹¹

$$\mathbf{R}, M \rightarrow \mathbf{R} + \mathbf{r}_M, m_M, \quad (6)$$

where \mathbf{r}_M is one of the N_p normal system lattice vectors within a supercell. The range of m_M is the possibly variable number of orbitals in each normal unit cell.

The unfolded spectral weight is given by¹¹

$$W^{\mathbf{K}J}(\mathbf{G}) = \frac{1}{N_p} \sum_{MN} C_N^{\mathbf{K}J*} U_{NM}(\mathbf{k}) C_M^{\mathbf{K}J}, \quad (7)$$

where $\mathbf{k} = \mathbf{K} + \mathbf{G}$, and

$$U_{NM}(\mathbf{k}) = \sum_{\mathbf{r}} e^{i\mathbf{k}\cdot(\mathbf{r}-\mathbf{r}_M)} S_{0N,\mathbf{r}m_M}, \quad (8)$$

which is a particular Fourier sum of overlap integrals that encapsulates the unfolding information. We shall call it the *unfolding matrix*. A convenience of this unfolding formula is that it does not require the definition of a virtual crystal for its implementation.

Noting the similarity between $U(\mathbf{k})$ and $S(\mathbf{K})$, we write partial unfolded orbital weights as

$$W_N^{\mathbf{K}J}(\mathbf{G}) = \frac{1}{N_p} \Re \left\{ C_N^{\mathbf{K}J*} \sum_M U_{NM}(\mathbf{k}) C_M^{\mathbf{K}J} \right\}, \quad (9)$$

so that $W^{\mathbf{K}J}(\mathbf{G}) = \sum_N W_N^{\mathbf{K}J}(\mathbf{G})$. We can verify that the unfolding matrix is hermitean, so that the spectral weights are real. This can be shown by writing $S_{0N,\mathbf{r}m_M}$ as $S_{\mathbf{r}_N n_N, \mathbf{r}m_M}$, and using the symmetry properties of overlap integrals. Another point to check is the special case of an orthonormal basis set. We can easily see that orthogonality implies that $S_{0N,\mathbf{r}m_M} = \delta_{\mathbf{r},\mathbf{r}_N} \delta_{n_N, m_M}$, from which we obtain the simpler result,¹⁰

$$U_{NM}(\mathbf{k}) = e^{i\mathbf{k}\cdot(\mathbf{r}_N - \mathbf{r}_M)} \delta_{n_N, m_M}. \quad (10)$$

The main numerical task pertains to the unfolding matrix, Eq. (8). First, there is a sum over the infinite set of lattice vectors \mathbf{r} , but the actual set is sharply restricted by the range of overlap integrals. Second, it must be noted that the overlap integral $S_{0N,\mathbf{r}m_M}$ is equivalent to one in the form of $S_{0N,\mathbf{R}M'}$, as given by the electronic structure code. The supercell and normal cell lattice vectors are related by $\mathbf{r} = \mathbf{R} + \mathbf{r}_i$, where \mathbf{r}_i is a normal lattice vector within a supercell, while the orbital index M' is determined by the pair of \mathbf{r}, m_M .

It is useful to have sum rules to verify the results of our calculations. By using Eq. (5), we can prove the sum rule,

$$\sum_{\mathbf{G}} W^{\mathbf{K}J}(\mathbf{G}) = 1. \quad (11)$$

Another practical sum rule is

$$\sum_J W^{\mathbf{K}J}(\mathbf{G}) = \frac{N_b}{N_p}, \quad (12)$$

where the right hand side is just the average number of basis orbitals in the primitive unit cell of the normal system. This sum rule is a consequence of the properties of the spectral function.

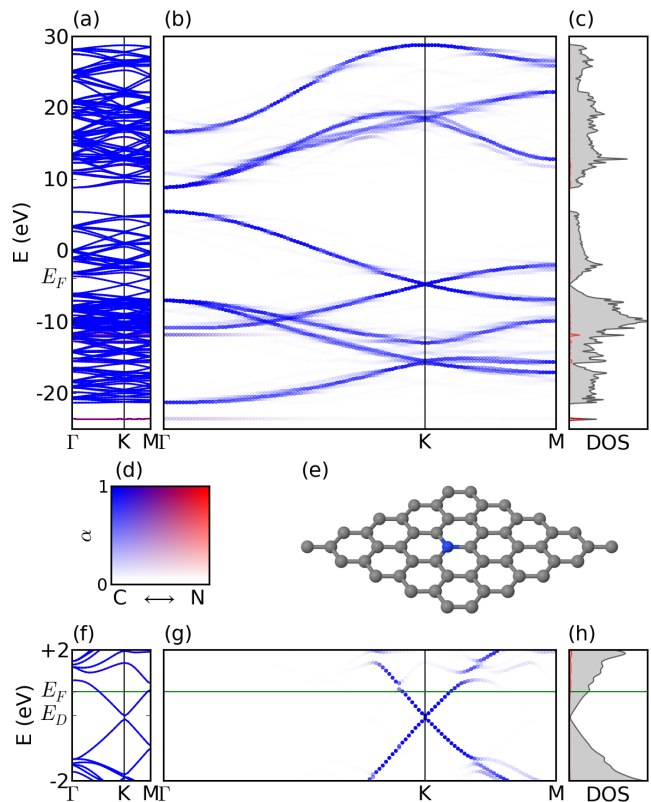


FIG. 2. (Color online) (a) Band structure of nitrogen-doped graphene obtained from supercell calculations. (b) Unfolded bands in the normal Brillouin zone. (c) Total DOS and PDOS of nitrogen orbitals. (d) Color map used in band structure plots. (e) The 5×5 unit cell with a nitrogen at the center. (f-h) Band structure and DOS plotted in a window centered on the Dirac point. Fermi level is seen to have shifted because of doping by the extra electron of nitrogen. There is a small band gap opening at the Dirac point.

III. RESULTS AND DISCUSSION

A. Perfect graphene

Band structure of perfect graphene provides a good testing ground for our numerical procedure, since we know exactly what to expect. Furthermore, it allows us to measure the computational load of the unfolding procedure, which is about the same in all cases that we consider.

We first explain our approach to visualization of band structures using the additional data contained in the unfolded spectral weights and orbital populations.¹⁶ In our 2D plotting package, we can specify colors and transparency in terms of parameters r, g, b and α , respectively, all in the 0–1 range.¹⁷ Hence in the rgb color space (0,0,0) and (1,1,1) represent black and white, respectively, which are visible or invisible on a white background. The α parameter controls transparency, so that $\alpha = 0$ is completely transparent and thus invisible, and $\alpha = 1$ is com-

pletely opaque. We adopt a simple scheme and always decompose the orbital contributions into only two sets, which are represented by blue (0,0,1) and red (1,0,0), respectively. We then use the normalized weighted average of the colors to represent mixing of the two sets, and set α equal to the total spectral weight, which results in the color map shown in Fig. 1(d). It is possible to partition the orbitals into more than two sets but the color maps become more complicated. We must mention that this continuous range of colors is unnecessary for the present case of perfect graphene, where the weights turn out to be zero or unity, but it will definitely be needed for defective graphene.

Figure 1(a) shows the band structure, using 25 k points along Γ KM path in the SBZ. We have assigned our two pure colors to the two sets consisting of $2s, 2p_x, 2p_y$ and $2p_z$ orbitals, respectively. This has made the σ and π bands to appear in these colors, since they are mutually orthogonal in graphene. However, because of heavy folding the bands are difficult to recognize.

Figure 1(b) shows the unfolded bands. We make the calculations using the same 5×5 unit cell along the Γ KM path in the NBZ of graphene. As this path is five times longer than the one in SBZ, we use 121 k points. The expected bands of graphene have emerged, in blue and red, out of the complicated supercell bands, shown in light grey. Figures 1(f–h) show the same data as in Figs. 1(a–c), but in the important range of low energies.

B. Nitrogen impurity

We repeated similar electronic structure calculations for a 5×5 graphene supercell with a single nitrogen substitutional impurity. The results are shown in Fig. 2, where we used the same visualization approach discussed in Sec. III A, except that we have partitioned the orbital contributions according to the atoms, C and N. Here the continuous color map shows its usefulness. We note the appearance of the bound states below each of σ and π bands, because of the presence of nitrogen impurity.¹⁸ In addition, unfolding shows that the weights of these states have nonuniform distributions in the NBZ.

In Figs. 2(f–h) we show the data for the low energy spectrum. Because of doping by nitrogen, the Fermi level has shifted above the neutrality point. The presence of impurity has also caused a small gap to open at the Dirac energy.

C. Hydrogen adsorbate

Results of calculations for single hydrogen adsorbate on a 5×5 graphene supercell are shown in Fig. 3. A buckling of the graphene lattice near hydrogen, seen in Fig. 3(e), indicates the formation of an sp^3 defect. Such a defect effectively creates a π orbital vacancy, which manifests itself as a midgap state at the Fermi level.^{19,20} We

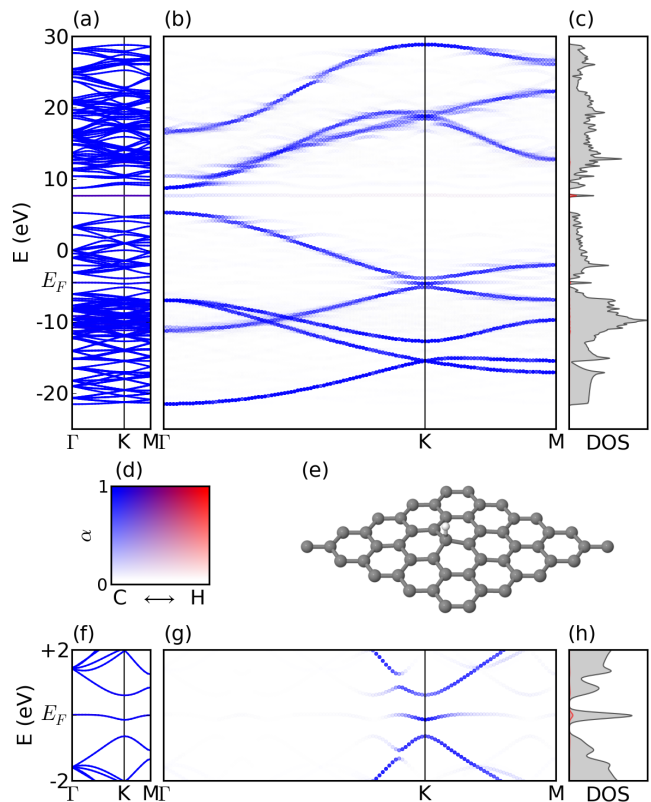


FIG. 3. (Color online) (a) Band structure of graphene with a hydrogen adsorbate obtained from supercell calculations. (b) Unfolded bands in the normal Brillouin zone. (c) Total DOS and PDOS of hydrogen orbital. (d) Color map used in band structure plots. (e) The 5×5 unit cell with a hydrogen at its center. A buckling of the lattice is visible near H. (f–h) Band structures and DOS plotted in a 4 eV window centered on the Dirac point.

can see the midgap state in all the band structure plots as well as the DOS plots. Moreover, most of the weight of the midgap band comes from carbon $2p_z$ orbitals. There is a bound state visible in the gap above the π bands with contributions from both C and H atoms, Figs. 3(a–c).²¹ We note, in Fig. 3(g), that the weight of the midgap band is accumulated near the K point, a fact that has also been observed in ARPES spectra of hydrogenated graphene.²²

D. Vacancy defect

Electronic structure calculation for graphene with a missing atom is shown in Fig. 4. Although not visible in Fig. 4(e), the relaxation of atoms indicates a Jahn-Teller distortion. There are four missing orbitals at the vacancy site, which can give rise to midgap bands, and other spectral changes.²³ Three midgap bands are clearly displayed in Figs. 4(f–h), where the use of the color map has also revealed the difference in their orbital decomposition. The two pure colors were assigned to two sets of

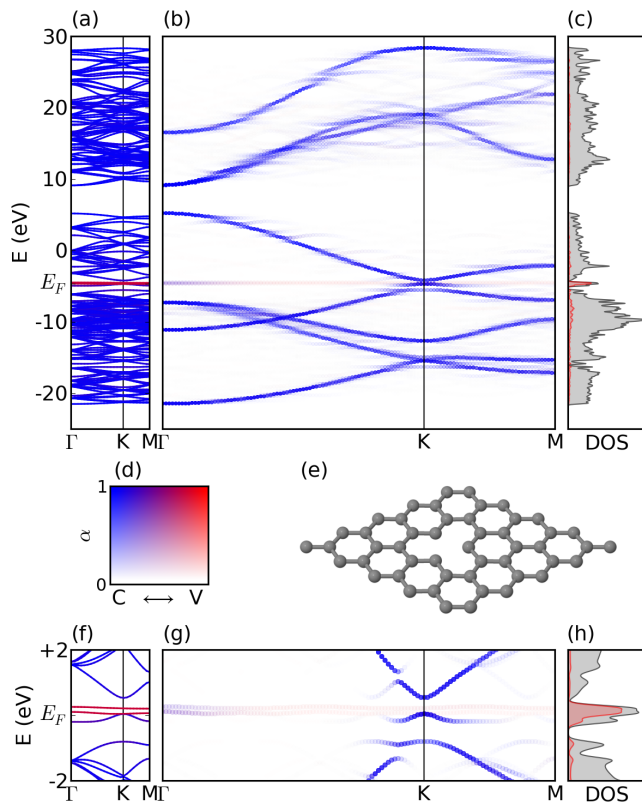


FIG. 4. (Color online) (a) Band structure of graphene with a vacancy obtained from supercell calculations. (b) Unfolded bands in normal Brillouin zone. (c) Total DOS and the PDOS of three carbon atoms bordering the vacancy site. (d) Color map used in band structure plots. (e) The 5×5 unit cell with a vacancy at its center. (f–h) Band structures and DOS in a 4 eV window centered on the Dirac point.

carbon atoms, ones nearest the vacancy site and the ones on the remaining sites.

In all cases, we checked that the sum rule, Eq. (12), holds. For pure graphene, or nitrogen impurity, the sum adds up to $N_b/N_p = 200/25 = 8$, while for hydrogen and vacancy defects it adds up to $201/25 = 8.04$, and $196/25 = 7.84$, respectively.

ACKNOWLEDGMENTS

I have greatly benefited from discussions with A. Grüneis.

* mfarjam@ipm.ir

¹ A. H. Castro Neto, F. Guinea, N. M. R. Peres, K. S. Novoselov, and A. K. Geim, *Rev. Mod. Phys.* **81**, 109 (2009).
² P. R. Wallace, *Phys. Rev.* **71**, 622 (1947).
³ K. S. Novoselov, A. K. Geim, S. V. Morozov, D. Jiang, Y. Zhang, S. V. Dubonos, I. V. Grigorieva, and A. A. Firsov, *Science* **306**, 666 (2004).
⁴ K. S. Novoselov, A. K. Geim, S. V. Morozov, D. Jiang, M. I. Katsnelson, I. V. Grigorieva, S. V. Dubonos, and A. A. Firsov, *Nature* **438**, 197 (2005).
⁵ Y. Zhang, Y. W. Tan, H. L. Stormer, and P. Kim, *Nature* **438**, 201 (2005).
⁶ D. Usachov, O. Vilkov, A. Grüneis, D. Haberer, A. Fedorov, V. K. Adamchuk, A. B. Preobrajenski, P. Dudin, A. Barinov, M. Oehzelt, C. Laubschat, and D. V. Vyalikh, *Nano Lett.* **11**, 5401 (2011).
⁷ O. V. Yazyev and L. Helm, *Phys. Rev. B* **75**, 125408 (2007).
⁸ P. B. Allen, T. Berlijn, D. A. Casavant, and J. M. Soler, *Phys. Rev. B* **87**, 085322 (2013).
⁹ T. B. Boykin and G. Klimeck, *Phys. Rev. B* **71**, 115215 (2005); T. B. Boykin, N. Kharche, G. Klimeck, and

M. Korkusinski, *J. Phys.: Condens. Matter* **19**, 036203 (2007).
¹⁰ W. Ku, T. Berlijn, and C.-C. Lee, *Phys. Rev. Lett.* **104**, 2010 (2010).
¹¹ C.-C. Lee, Y. Yamada-Takamura, and T. Ozaki, *J. Phys.: Condens. Matter* **25**, 345501 (2013).
¹² V. Popescu and A. Zunger, *Phys. Rev. Lett.* **104**, 236403 (2010); *Phys. Rev. B* **85**, 085201 (2012).
¹³ A. N. Rudenko, F. J. Keil, M. I. Katsnelson, and A. I. Lichtenstein, *Phys. Rev. B* **88**, 081405(R) (2013).
¹⁴ B. Aradi, B. Hourahine, and T. Frauenheim, *J. Phys. Chem. A* **111**, 5678 (2007). We used the mio-0-1 set of Slater-Koster parameters, obtained from <http://www.dftb.org>.
¹⁵ M. Elstner, D. Porezag, G. Jungnickel, J. Elsner, T. Frauenheim, S. Suhai, and G. Seifert, *Phys. Rev. B* **58**, 7260 (1998).
¹⁶ See also (the supplementary of) T. Berlijn, D. Volja, and W. Ku, *Phys. Rev. Lett.* **106**, 077005 (2011).
¹⁷ We use the matplotlib package: J. D. Hunter, *Computing in Science and Engineering* **9**, 90 (2007).
¹⁸ Ph. Lambin, H. Amara, F. Ducastelle, and L. Henrard,

- Phys. Rev. B **86**, 2012 (2012).
- ¹⁹ T. O. Wehling, M. I. Katsnelson, and A. I. Lichtenstein, Phys. Rev. B **80**, 085428 (2009).
- ²⁰ M. Mirzadeh and M. Farjam, J. Phys.: Condens. Matter **24**, 235304 (2012).
- ²¹ M. Farjam, D. Haberer, and A. Grüneis, Phys. Rev. B. **83**, 193411 (2011).
- ²² D. Haberer, L. Petaccia, M. Farjam, S. Taioli, S. A. Jafari, A. Nefedov, W. Zhang, L. Calliari, G. Scarduelli, B. Dora, D. V. Vyalikh, T. Pichler, C. Wöll, D. Alfè, S. Simonucci, M. S. Dresselhaus, M. Knupfer, B. Büchner, and A. Grüneis, Phys. Rev. B **83**, 165433 (2011).
- ²³ B. R. K. Nanda, M. Sherafati, Z. S. Popović, and S. Satpathy, New J. Phys. **14**, 083004 (2012).